

# Sodium in Cu(In, Ga)Se<sub>2</sub> Solar Cells: To Be or Not to Be Beneficial

Ava Karami, Marcin Morawski, Heiko Kempa, Roland Scheer, and Oana Cojocaru-Mirédin\*

In this work, the dual effect of Na in the copper indium gallium diselenide (CIGS) absorber is studied. Na doping exhibits a drastic improvement of the cell efficiency mainly by an increase in the open-circuit current and fill factor. However, when the Na content is too high, it can deteriorate the cell properties and performance. Nonetheless, it is still beneficial when compared with a cell without Na inside. Here, we therefore use electron backscatter diffraction, atom probe tomography, and admittance spectroscopy to understand why Na starts to deteriorate the properties when inserted excessively. More exactly, it is shown that a moderate addition of Na strongly decreases the open-circuit voltage ( $V_{OC}$ ) deficit, whereas the opposite happens when the Na content is too high. Interestingly, this cell with deteriorated  $V_{OC}$  value and characterized by a very high Na content exhibits a high density of not only grain boundaries and dislocations but also of Na-rich clusters. These clusters may host a high concentration of deep defects and trap the electrons within the CIGS bulk. At this stage, Na still has its beneficial effects, but the cell properties start to deteriorate compared to the cell with a moderate content of Na, especially when found as clusters in the bulk. In conclusion, this work clearly demonstrates the dual effect of Na in the CIGS absorber.

## 1. Introduction

Copper indium gallium diselenide (CIGS) based thin-film solar cells are now one of the most promising absorbers to alternate the conventional silicon-based modules.<sup>[1]</sup> This compound semiconductor with I-III-VI<sub>2</sub> chalcopyrite crystal structure attained interest due to its many favorable material characteristics such as tunable bandgap and high optical absorption coefficient ( $\geq 10^5 \text{ cm}^{-1}$ ), achieved in layers as thin as 2  $\mu\text{m}$ .<sup>[1]</sup> These thin polycrystalline absorber layers contain many grain boundaries (GBs), which are believed to be electrically detrimental to the cell performance by acting as active recombination centers for free charge carriers<sup>[2]</sup> and reducing the open-circuit voltage ( $V_{OC}$ ).<sup>[3–5]</sup> Yet, the record efficiency of 23.4%<sup>[6]</sup> of the polycrystalline absorbers confirms their superiority to the monocrystalline counterparts<sup>[7]</sup> and might suggest that the GBs are not that harmful to the device after all.<sup>[8]</sup>


Various studies have been conducted to explain the benign effect of GBs on the CIGS cell efficiency. The cause is mainly attributed to the passivation effect at GBs by the incorporation of alkali dopants in the CIGS absorber layer.<sup>[9,10]</sup> Na-doping has exhibited a drastic improvement in the cell conversion efficiency of CIGS thin-film solar cells steadily rising from 8.8%<sup>[11]</sup> to 16.8%<sup>[11]</sup> when Na is added. In particular, the  $V_{OC}$  and fill factor (FF) are strongly enhanced due to decreased interfacial recombination.<sup>[8,12,13]</sup> Moreover, the short circuit current ( $J_{SC}$ ) increases because Na is not only found at the GBs but also diffuses inside the CIGS bulk.<sup>[14,15]</sup> This leads to an increase in the acceptor density ( $p$ ) and hence, to a higher conductivity of the charge carriers in the bulk.<sup>[16,17]</sup> The depletion region width is also 3 times smaller in the presence of Na in the absorbers compared to the ones without Na inside.<sup>[18]</sup>

Although numerous studies exist on the “Na effect” in CIGS, they have been ambiguous when Na was inserted in too high content. These few studies mentioned that when Na is found in too high extent the cell performance is degraded.<sup>[19,20]</sup> The main reasons given were either the reduction of the In–Ga interdiffusion (stronger Ga gradient in the absorber with direct implications on the optoelectronic properties of the absorber) or the formation of a new Na<sub>2</sub>CO<sub>3</sub> phase on the absorber surface leading to strong interfacial recombination (either the presence of a

A. Karami, O. Cojocaru-Mirédin  
RWTH Aachen  
I. Physikalisches Institut IA  
Sommerfeldstraße 14, 52074 Aachen, Germany  
E-mail: oana.cojocaru-miredin@inatech.uni-freiburg.de

M. Morawski, H. Kempa, R. Scheer  
Martin Luther-Universität Halle-Wittenberg  
Institut für Physik  
FG Photovoltaik, 06099 Halle, Germany

O. Cojocaru-Mirédin  
Albert-Ludwigs Universität Freiburg  
INATECH  
Emmy-Noether-Straße 2, 79110 Freiburg, Germany

 The ORCID identification number(s) for the author(s) of this article can be found under <https://doi.org/10.1002/solr.202300544>.

© 2023 The Authors. Solar RRL published by Wiley-VCH GmbH. This is an open access article under the terms of the Creative Commons Attribution-NonCommercial-NoDerivs License, which permits use and distribution in any medium, provided the original work is properly cited, the use is non-commercial and no modifications or adaptations are made.

DOI: 10.1002/solr.202300544

Ga rich phase due to reduced Ga mobility or the formation of Na rich phases on the absorber surface when Na is inserted through the NaF post-deposition treatment).<sup>[19,20]</sup> Hence, despite all the numerous studies done to understand the Na effect,<sup>[13,21–23]</sup> none of these studies mentioned to which extent Na must be incorporated to reach an optimum performance and what exactly happens when Na is inserted in too-high content.

Moreover, in most of the existing studies, the common strategy to incorporate the Na was mainly post-deposition treatment (PDT), in which Na is effectively supplied by evaporation of the NaF precursor layer at a low-temperature Se ambient. Within this incorporation method, no Na is present during recrystallization and the exact dosage of Na in the absorber is ambiguous since very often some of the Na remains at the CIGS surface either as a NaF compound or as a new NaInSe<sub>2</sub> compound.<sup>[24,25]</sup>

Therefore, in this work, a new incorporation strategy is established to supply a quantified amount of Na into the CIGS absorber. In this investigation, NaF precursor layers with different thicknesses are deposited before the absorber growth onto the Mo back contact. This work provides a comprehensive study of how Na affects the microstructure and electrical properties of the absorber when found not only in moderate content but also in very high content. Moreover, it provides an exact Na quantification necessary for optimum cell efficiency. For that, atom-probe tomography (APT) is used since it allows us to quantify Na and elemental content in three dimensions and down to the atomic scale. Moreover, the composition obtained by APT is corroborated with the structural and electrical properties by employing electron backscatter diffraction (EBSD) and admittance spectroscopy (AS). Hence here we elucidate the possible dual effect of Na in absorber layers of a CIGS solar cell.

## 2. Experimental Section

### 2.1. CIGS Solar Cell Fabrication

The NaF precursor layers with thicknesses of 0, 6, and 14 nm are co-evaporated onto Mo-coated soda-lime glass (SLG) substrate before the CIGS deposition at the nominal substrate temperature of 25 °C. This variation in the thickness of the nominal precursor layer is for adjusting the Na content in the CIGS absorber layer. A 110 nm thick SiN<sub>x</sub> diffusion barrier was deposited in between Mo back contact and SLG substrate to prevent the diffusion of supplementary Na, O, and K from the substrate into the absorber layer. The CIGS absorber layers of 1.7 μm thickness are grown in one identical process onto the NaF precursor layer using the 3-stage co-evaporation recipe invented by Gabor et al.<sup>[26]</sup> The fabrication of the absorber layer has been conducted by co-evaporation of Cu, In, Ga, and Se from elemental sources, within a vacuum environment. The final compositional ratios measured by energy dispersive X-Ray analysis (EDX) for the CIGS absorber layers investigated in this work, were [Cu]/([In] + [Ga]) = 0.92 and [Ga]/([In] + [Ga]) = 0.29. The sodium concentration was determined by glow discharge optical emission spectroscopy (GDOES) averaging the Na depth profile over thickness.

The fabrication of solar cell devices was completed by chemical bath deposition of a CdS buffer layer, an RF-sputtered



**Figure 1.** Schematic layer stack of the CIGS solar cell. The CIGS absorber layer with a thickness of about 2 μm is doped with Na by depositing a NaF precursor layer onto the substrate, before CIGSe evaporation.

i-ZnO/ZnO: Al bilayer front contacts, and finally, a Ni/Al front contact grid to improve the current collection. **Figure 1** shows a schematic layer stack of the produced CIGS solar cell with varying thicknesses of NaF precursor layer deposited onto a Mo-coated substrate, to adjust the content of Na incorporated into the CIGS layer.

The three cells that will be studied in this work are called Na-0 (no NaF layer was present between the Mo and CIGS), Na-6 (6 nm NaF), and Na-14 (14 nm NaF).

### 2.2. Characterization Methods

The fabricated CIGS films were analyzed using different characterization techniques. The device performance was determined by current–voltage (*I*–*V*) measurements under illumination with AM1.5G simulated spectrum using standard test conditions. The structure and composition properties of the CIGS thin films were investigated by EBSD and APT.

From the minimum of the GDOES [Ga]/([In] + [Ga]) depth profile, the CIGS bandgap energy was calculated. These bandgap energy values were then confirmed by external quantum efficiency curves evaluating the minimum of the first derivative dEQE/dE. Note that due to the simultaneous deposition of CIGS for all Na samples in this study, the band gap came out identical within the typical error limits.

Samples for EBSD analysis were prepared using a dual-beam focused ion beam (FIB)/scanning electron microscope (SEM) mounted in FEI Helios NanoLab 650, with the EDAX detector using a DigiView 5 camera. Before the EBSD measurements, the coating layers including ZnO and CdS were removed by FIB with a Ga<sup>+</sup> beam to obtain a smooth CIGS surface, which is essential for EBSD measurements. This avoids the appearance of topographic artifacts and provides Kikuchi patterns with higher qualities. The cleaned regions with the size of 15 × 15 μm were obtained in two steps. At first, the surfaces are cleaned using high voltage and current of 30 kV and 2.5 nA, and then with lower voltage and current of 5 kV and 43 pA, to reduce the contamination and amorphization induced by higher current and voltages. Then EBSD was performed with the SEM electron beam at the voltage and current of 20 kV and 1.6 nA using 4 × 4 binning resolution, 0.05 μm step size, and a tilt angle of 70°.

The results were processed by orientation imaging microscopy (OIM) data analysis software.

To prepare the samples for quantitative APT measurements, they need to be sharpened into a thin needle shape with a diameter of less than 100 nm at the apex. The preparation method of thin needles is done by the “lift-out method”,<sup>[27]</sup> a very well-established technique using a dual-beam FIB. The ion beam column allows Ga<sup>+</sup> ion beam milling at an accelerating voltage of 16 kV. The CIGS lamella is placed on a Si coupon by Pt deposition in the FIB. The radii of the APT sample are decreased by “annular milling” until the sample reaches a diameter of <60 nm. Finally, the sample obtains a tip shape and has to be cleaned under a small voltage of 5 kV to minimize the contamination with Ga<sup>+</sup>. After the preparation procedure, these samples are measured with the APT to reveal the 3D distributions of the elements.

The APT measurements are performed at temperatures between 20 and 50 K (cryogenic temperature), to avoid the migration of atoms to the surface of the needle-shaped specimen. The UV laser pulses with the wavelength of 355 nm and the laser energy of 3 pJ (250 kHz laser frequency) are applied to the tip. This can generate local heating on the APT tip and increase the temperature from 40 K (set temperature) to about 100 K.<sup>[28]</sup>

Admittance spectroscopy was conducted with an Agilent E4980A LCR meter from 1 kHz to 1 MHz with AC signal amplitude of 20 mV. The sample was bonded and mounted on a temperature chuck in vacuum. The temperature has been varied in 10 K steps from 70 to 300 K using a closed-cycle helium cryostat.

### 3. Results

**Figure 2** shows the *I*–*V* curves for the three CIGS cells studied in this work. The difference between them comes only from the difference in NaF thicknesses. An obvious change in the *V*<sub>OC</sub> and *J*<sub>SC</sub> values when adding Na-dopants is observed. The Na-6 sample is experiencing an increase of *V*<sub>OC</sub> and FF of about 120 mV and 6%, respectively (while *J*<sub>SC</sub> stays almost the same when going from Na-0 to Na-6) proving as expected the positive impact of Na on the overall cell parameters and efficiency. Yet,

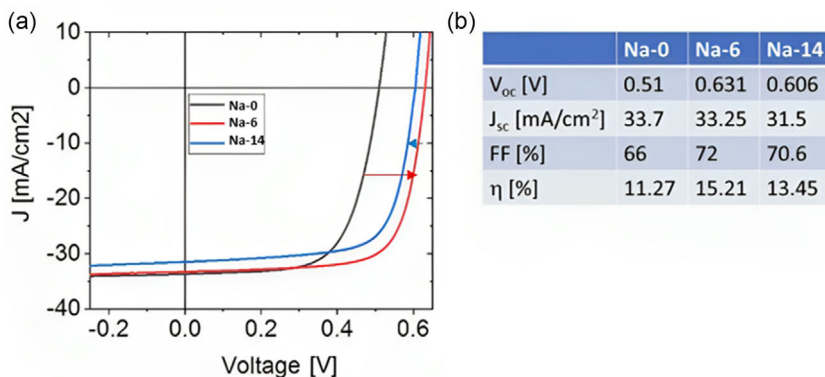


**Figure 2.** *I*–*V* curves for the three CIGS thin cells with different Na-amount in the absorber layer. a) As described in the experimental section the amount of Na in the absorber layer, corresponds to the different thicknesses of the NaF precursor layers. An obvious tendency of the *V*<sub>OC</sub> and *J*<sub>SC</sub> parameters regarding the content of Na is shown. The sample with a moderate content of Na-dopants in the CIGS absorber is experiencing an increase in the *V*<sub>OC</sub>. Whereas with the further increase of the Na content in the absorber, the *V*<sub>OC</sub> undergoes a significant decrease. b) Cell parameters of the three solar cells for Na-0, Na-6, and Na-14.

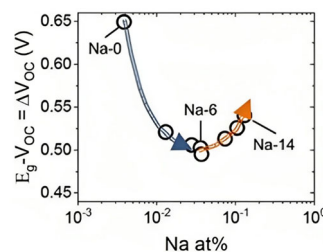


**Figure 3.** *V*<sub>OC</sub> deficit as a function of the Na content in the CIGS absorber layer. The moderate addition of Na-dopants into the absorber material appears to yield a decrease of around 150 mV in *V*<sub>OC</sub> deficit, while with higher content of Na-dopants, the *V*<sub>OC</sub> deficit experiences an increase of around 50 mV.

with the further increase of the Na content in the absorber (from Na-6 to Na-14), the *V*<sub>OC</sub> undergoes a decrease in all cell parameters, i.e., of 25 mV for *V*<sub>OC</sub>, of 1.75 mA cm<sup>−2</sup> for *J*<sub>SC</sub> and of 1.5% for FF. This implies that Na starts to have a negative effect on the overall cell parameters and, hence, cell efficiency when found in too high content.

**Figure 3** shows the *V*<sub>OC</sub> deficit as a function of the Na content in the CIGS absorber layer. This *V*<sub>OC</sub> deficit is given by the difference between the theoretical maximum open-circuit voltage *V*<sub>OC,max</sub> (at 0 K) and the actual open-circuit voltage *V*<sub>OC</sub>. Hence, the *V*<sub>OC</sub> deficit can be related to the band gap and the actual open-circuit voltage *V*<sub>OC</sub> through the equation:

$$V_{OC} \text{ deficit} = \frac{E_g}{q} - V_{OC} \quad (1)$$

where *q* represents the elementary charge.

It is indeed well known that the actual *V*<sub>OC</sub> is strongly negatively impacted by the presence of internal interfaces in devices due to the GB recombination phenomenon.<sup>[9]</sup> Charged defects are believed to act as active recombination centers that reduce *V*<sub>OC</sub> and degrade the cell efficiency. Yet, the interfaces in CIGS are characterized by a high degree of complexity, with a wide range of material properties that can vary significantly from

one region to another. For instance, the GBs can exhibit a wide range of properties, such as chemical, structural, and electronic properties (carrier concentration, recombination rate, and defect density)<sup>[8,29–31]</sup> which will strongly impact the  $V_{OC}$  deficit. Hence, the typical  $V_{OC}$  deficit for high-performant CIGS solar cells values falls in the range of 0.3 to 0.5 V.<sup>[8]</sup>

Here the minimum  $V_{OC}$  deficit was registered for the sample containing a moderate Na content in the absorber material (0.5 V), while with a higher content of Na-dopants, the  $V_{OC}$  deficit is experiencing an increase of around 35 mV. Moreover, the highest  $V_{OC}$  deficit value of 0.65 V was registered for the Na-free sample which proves again the necessity to insert Na-dopants to reduce the recombination losses in the cell. Other experiments showed that the Na-0 cell is indeed limited by interface recombination which can be deduced from the typical effects 1) extrapolated  $V_{OC}(0\text{ K}) < E_g/q$ <sup>[32]</sup> and 2) slope  $dV_{OC}/dt < 0$ .<sup>[33]</sup> The two other cells Na-6 and Na-14 did show  $V_{OC}(0\text{ K}) \approx E_g/q$  and  $dV_{OC}/dt > 0$  which proves bulk recombination (and not interface recombination) is the limiting process of these solar cells.<sup>[33]</sup>

Besides Na-0, Na-6, and Na-14, there are other data points shown in Figure 3, which are related to the samples with different content of Na inside. These samples are not investigated and not discussed in this work, due to the very time-consuming preparation technique for the APT samples.

Figure 4 gives the admittance spectra at varied temperatures for the sample Na-6 which is typical for the Na precursor series of this study. One can identify several characteristic capacitance densities C1–C3 marked by dashed lines. While C2 corresponds to the space charge capacitance  $C_{SCR}$ , C1 is the series connection of the SCR with the back-contact barrier capacitance.<sup>[34]</sup> The capacitance increase from C2 to C3 is due to a deep defect level which is crossed by the Fermi level in the SCR.<sup>[35]</sup> Since the defect contribution will show up as a parallel capacitance concerning the SCR capacitance, we will consider the quantity  $\Delta C = C3 - C2$  which we interpret as a measure of the deep defect density.

Table 1 gives the data from the admittance evaluation for the samples Na-0, Na-6, and Na-14. It can be seen that  $C_{SCR}$  increases monotonously which is interpreted as an increase in doping density  $N_A$  upon Na doping. This CIGSe doping effect by Na is in accordance with the literature and has been explained by a defect model.<sup>[36]</sup> With higher Na concentration, also the  $\Delta C$  increases. This capacitance contribution, we interpret as an increase in deep

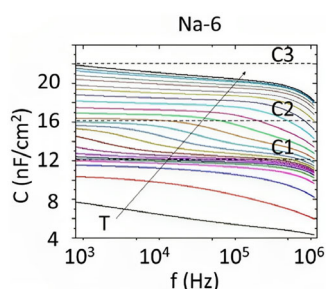


**Figure 4.** Representative admittance spectra for different temperatures (70–300 K in 10 K steps) for sample Na-6. C1–C3 indicate characteristic capacitance values which are interpreted in the text.

**Table 1.** Evaluation of admittance spectra according to Figure 4.  $C_{SCR}$  equals C2 in Figure 4 and denotes the space charge capacitance.  $N_A$  is the absorber doping which has been calculated from  $C_{SCR}$  assuming a one-sided junction.  $\Delta C$  gives the capacitance difference C3–C2.

Sample	$C_{SCR}$ [nF cm <sup>-2</sup> ]	$N_A$ [cm <sup>-3</sup> ]	$\Delta C$ [nF cm <sup>-2</sup> ]
Na-0	4.6	1.76E + 14	1.8
Na-6	16	2.12E + 15	5
Na-14	32	8.5E + 15	14

defect concentration. Simulation points out that these defects are located at around midgap, perhaps with some energy distribution which is not resolved in the experiments. Due to their deep location in the bandgap, the step in the C(f) plot is not complete. Hence, an activation energy cannot be determined.

EBS measurements are performed to investigate the Na effect on the microstructure of the CIGS absorber layer. The EBSD pattern quality map in Figure 5a shows that in Na-free CIGS absorber 51% of the GBs detected in the blue-colored lines are random high-angle GBs (RHAGBs) with the misorientation angle greater than about 15° and 48% of the identified GBs highlighted in yellow and green-colored lines are  $\Sigma 3$  twin boundaries (TBs), 60°–<221> and 71°–<110>. The presence of a moderate amount of Na (sample Na-6) increases the fraction of RHAGBs to 58%, which further increases to 70% (Figure 5b) for the Na-14 sample. Subsequently, the proportion of TBs decreases as the content of Na increases. This is due to the bulk-like behavior of the TBs, as claimed in most of the previous studies. Despite the RHAGBs, the  $\Sigma 3$  TBs exhibit a high degree of symmetry, which prevents them from accepting Na elements, while the RHAGBs contain a high density of gap states and can adopt easily the Na-dopants.

The grain sizes are also impacted by the content of Na, as shown in Figure 5c. The average grain size is reduced from 1.64  $\mu\text{m}$  for the cell with no dopants to 1.17 and 1.06  $\mu\text{m}$  for the cells with moderate (Na-6) and high content of Na (Na-14), respectively. These findings demonstrate that Na reduces the grain size of the CIGS strongly. Yet, as mentioned previously the Na reduces the fraction of twin boundaries too. This suggests that contrary to the twin boundaries, the RHAGBs decorated by Na are more rigid and less mobile during the growth of the CIGS absorber layer leading to smaller grain sizes of the crystals.

The reduction of grain sizes by incorporation of Na-dopants has been previously reported by various studies,<sup>[37–39]</sup> but our findings regarding the lower fraction of TBs by adding more Na dopants are novel and have not been mentioned in any literature before. Our previous works explain that most of the twin boundaries do not show any variation in composition and no alkali dopant segregation, which revealed their bulk-like behavior.<sup>[8,31,40,41]</sup> Na and the other alkali atoms are mainly discovered at random GBs. The absence of Na at TBs could also be related to the disability of the current techniques in measuring the Na content at very low levels.<sup>[42]</sup>

To investigate the effect of Na doping on the texture of CIGSe, the pole figures of the three samples are plotted (see Figure S1, Supporting Information). Figure S1 (Supporting Information)

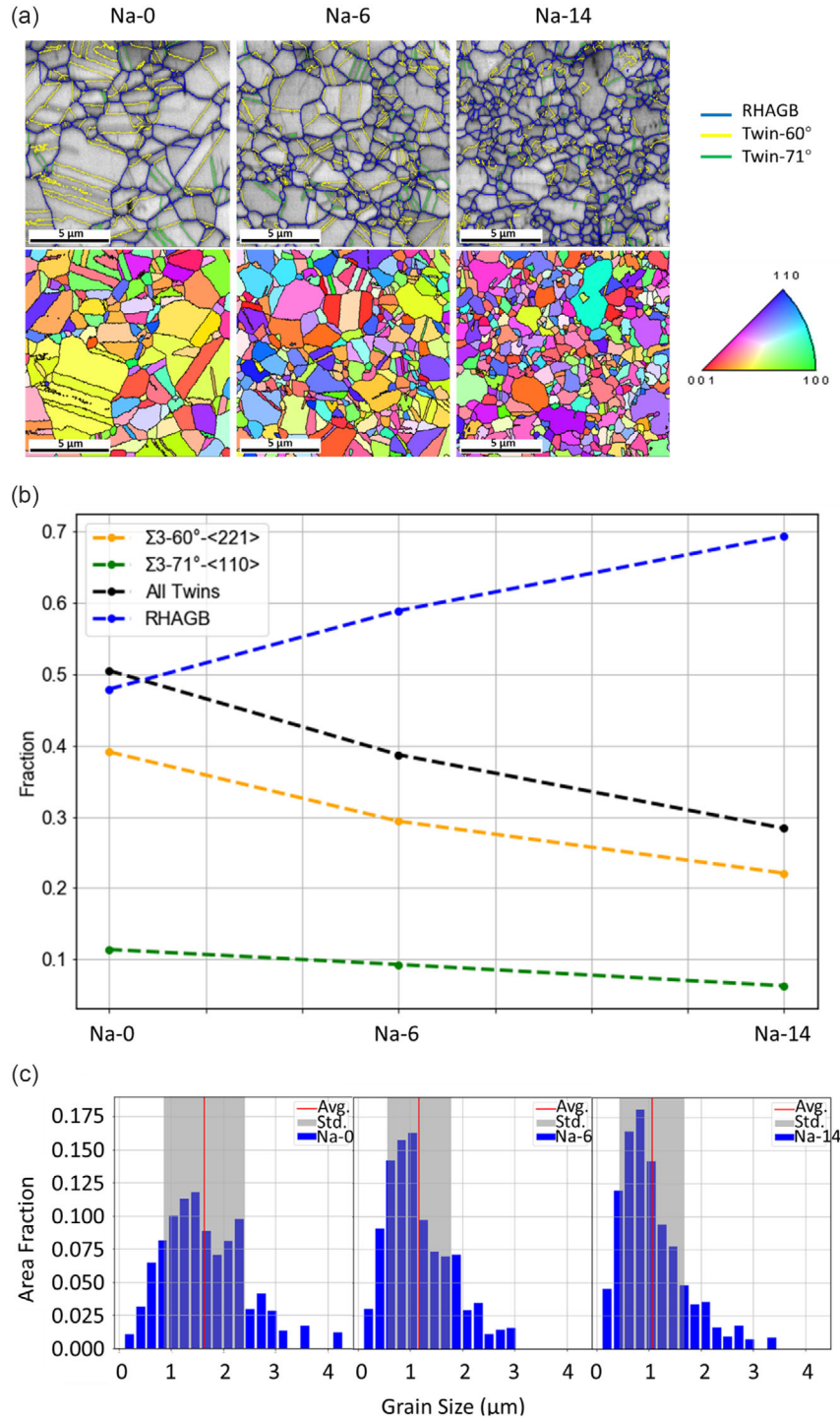


**Figure 5.** EBSD investigations revealed the microstructure properties of the GBs influenced by the presence of Na-dopants during the absorber growth for the samples Na-0, Na-6, and Na-14 respectively. a) EBSD grain boundaries maps represent random high-angle (blue), twin 60° (yellow), and twin 71° (green) grain boundaries. b) EBSD inverse pole figures maps reveal the position of the GBs and the distribution of grains. c) Grain size distribution of the samples with no, moderate, and high Na-dopants inside, respectively from left to right.

shows that a weak  $\langle 112 \rangle$ -texture is present in Na-0 and Na-6 samples, as represented by the symmetric structure in their pole figures. This weak  $\langle 112 \rangle$ -texture vanished as Na content increased further in the Na-14 sample, which indicates that the grain orientation becomes random when the Na content is strongly increased.

These results show that Na has a great impact on the CIGS microstructure and texture, but what about the GB composition?

To answer this question, Na and elemental composition have been investigated in each sample using APT. Figure 6a,b shows the 3D APT elemental map of the analyzed volume and the 1D

concentration profile of elements at the GB for the alkali-free CIGS absorber (Na-0 sample). The GB is found in the middle of the 3D map, where its position is highlighted (in blue) by an iso-composition surface made using a Cu iso-composition value of 19 at%. In agreement with our recent studies,<sup>[8,29–31,40,43]</sup> the Na is mainly localized at the GBs of the CIGS absorber layer. Moreover, linear defects decorated by Na and attributed to dislocations<sup>[40]</sup> are found in the CIGS absorber (see 3D map in Figure 6c).

The 1D concentration profile shows a strong Cu-depletion of 4.26 at%, in correlation with In and Se enrichment of  $\approx 3.1$  and

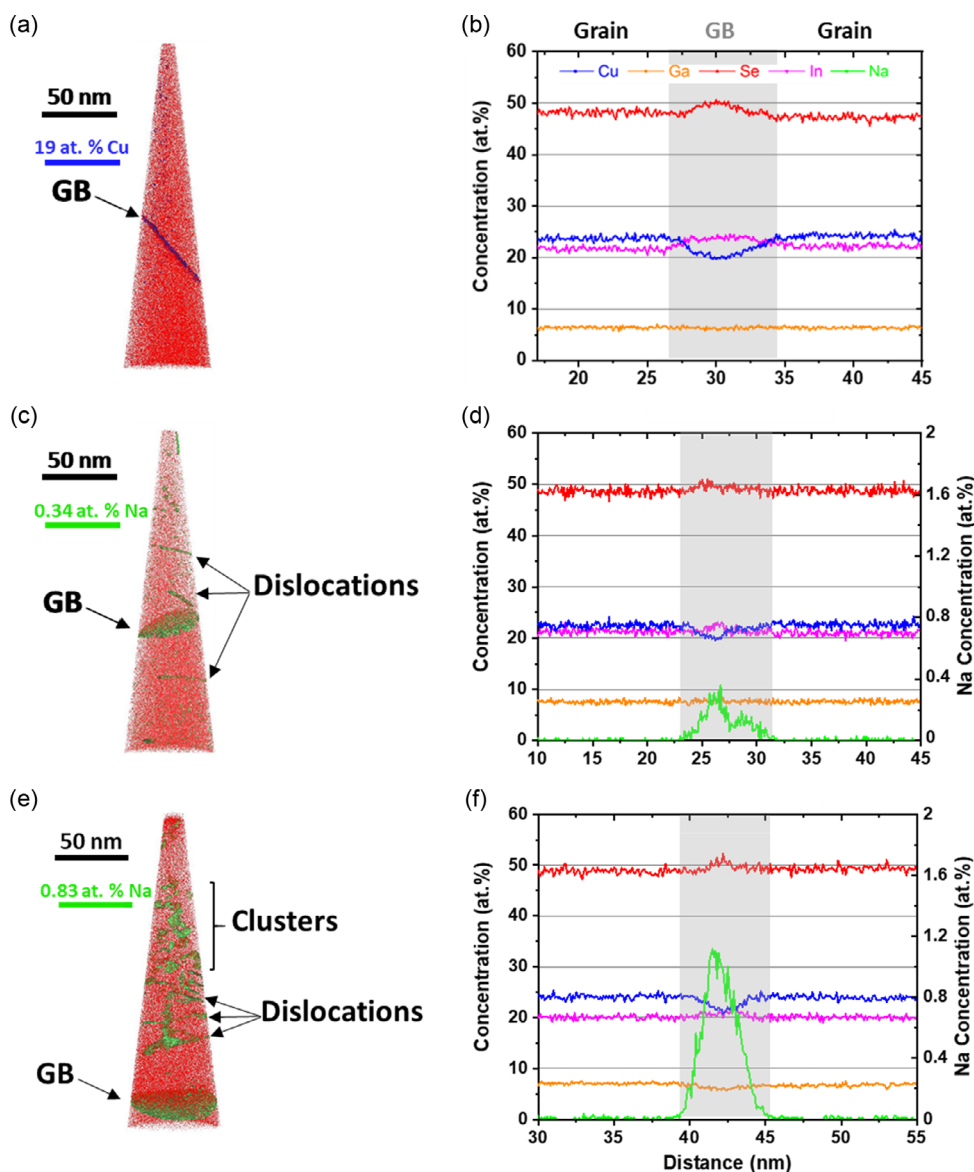


**Figure 6.** The chemical composition of GBs upon Na addition was determined by APT for the sample with No, moderate, and high content of Na from top to bottom, respectively. a) 3D APT map of the analyzed volume of the sample with No Na showing the presence of a GB. b) 1D concentration profile showing the composition of the grain and GB region (highlighted in gray). c) 3D elemental map of the sample with moderate content of Na showing the presence of one GB in the middle of the map and 5 different dislocations. d) 1D concentration profile of the sample doped by a moderate amount of Na showing a decrease in the magnitude in In-Cu anticorrelation, and Na accumulates at the GB position, in the range of 1 and 2 at%. e) 3D elemental map of the analyzed volume of the sample with the highest Na-dopants showing an enhanced content of GBs, dislocations, and clusters. f) 1D concentration profile of the sample doped by a high amount of Na showing a higher Na accumulation at the GB position, in the range of 1 to 2 at%.

≈ 2.5 at%, respectively (GB position highlighted in gray in the 1D concentration profiles). This In-Cu anticorrelation can be linked to the presence of Cu vacancies ( $V_{Cu}^-$ ) and In-on-Cu anti-site ( $In_{Cu}^{2+}$ ) defects.<sup>[8]</sup> Now by doping a moderate amount of Na (sample Na-6) in Figure 6c,d, the magnitude in In-Cu anticorrelation lowers (Cu depletion in the order of 2.46 at% and In and Se enrichment of 1.9 and 2.1 at%, respectively), and Na accumulates at the GB position, in the range of 1 to 2 at%. Interestingly, by further addition of Na-dopants into the absorber material (sample Na-14), besides the GB and dislocations, a high number density of clusters emerge in the APT 3D map (as shown in Figure 6e,f).

## 4. Discussion

### 4.1. Na Effect on Absorber Microstructure and Composition

A deeper analysis of the 1D concentration profiles shown in Figure 6 suggests that a close composition correlation between Na and Cu exists not only at the GBs but also in the grain interior (GI). To highlight that, we plot in Figure 7a the Cu composition at the GBs and in the GI for the NaF precursor series. A comparison allows us to identify  $\Delta Cu$  values for each sample where  $\Delta Cu$  gives the concentration difference between GI and GB. These  $\Delta Cu$  values are also given for CIGS solar cell samples with and without applying a NaF post-deposition treatment (PDT, see Figure 7b). It is visible that the  $\Delta Cu$  values are smaller when Na is present in the film (decrease from  $-4.26$  to  $-2.46/-2.69$  at% for the precursor films and from  $-8.49$  to  $-7.51$  at% for the PDT films, see Table 2). Thus, it appears that the addition of sodium reduces the Cu-depletion of the GBs.

If we consider the CIGS absorber a thermodynamically closed system where no loss takes place, then we can state that the missing atoms at the GBs may have been pushed back inside the GI. The change in the magnitude of  $\Delta Cu$  between Na-0 and Na-6 (and Na-14) suggests that interexchange exists between the GBs and the GI. Therefore, we believe that the smaller  $\Delta Cu$  of the sodium-doped films is the result of the migration of Cu atoms from the GBs to the GI when Na is introduced into CIGS

**Table 2.** Composition values for the Cu and Na elements inside the grains and at the GBs for each sample.

		Na Present during Recrystallization			Na coming from Na-PDT	
		Na-0	Na-6	Na-14	Alkali-free	NaF-PDT
Cu [at%]	Grain Interior (GI)	24.2	22.58	24.3	22.37	22.56
	Grain Boundary (GB)	19.94	20.12	21.61	13.87	15.05
	Delta ( $\Delta$ )	-4.26	-2.46	-2.69	-8.49	-7.51
Na [ppm]	Grain Interior (GI)		42	86		18
	Grain Boundary (GB)		1699	9244		11 225
	Delta ( $\Delta$ )		1657	9158		11 207

thin films. This we attribute to the replacement of Cu atoms by Na due to the relatively low formation energy of  $Na_{Cu}$  (0.40–0.60 eV).<sup>[36]</sup> Yuan et al.<sup>[44]</sup> as well as our recent results<sup>[8]</sup> explained that at temperatures  $T > 400$  °C first the Na atoms diffuse into the grain interior and replace Cu atoms. During the cooling process, the Na concentration in the GI is thermodynamically super saturated and Na atoms start to move back into the GBs leaving behind Cu vacancies  $V_{Cu}$  in the GI. Vice versa, the accumulation of Na at the GBs then leads to the back-diffusion of part of Cu atoms into the GI. The more Na accumulates at the GBs the more Cu from the GBs will be diffusing back inside the bulk (GI). This nicely fits with the findings from Figure 7a,b where the Cu content in the GI is increasing with increasing the Na content in the CIGS absorber layer for both Na-insertion procedures (for the NaF precursor and NaF PDT). Yet, interestingly we do not observe a gradual reduction of Cu content at the GBs with the Na addition as one would expect. This is because the Na effect at the GBs differs significantly from that inside the GI. The CIGS bulk (GI) is a well-ordered region with Na inserted either as an interstitial or as a lattice atom. In the latter case, the Na atom will replace either the Cu vacancy (but the content is generally low) or the Cu site, given that Cu interstitials have a very low formation energy within the CIGS bulk. However, the GB is a disordered region

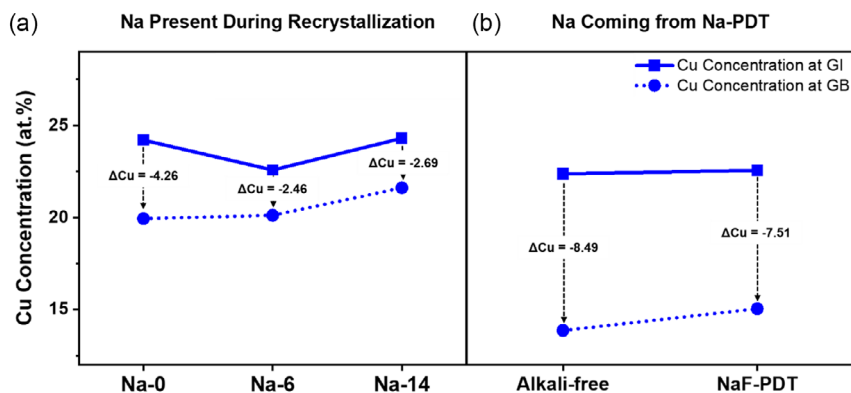


**Figure 7.** Copper and sodium compositional variations at the GI and GB within the absorber layers with different levels of Na content. a) Comparison of Cu-depletion magnitude in the CIGS samples grown under the presence of various Na content versus CIGS sample prepared using Na-PDT in b). Data in (b) originate from the work given in ref. [55]. The solar cells here consist of a ZnO/CdS/CIGS/Mo/ZrO<sub>2</sub> stacking structure, and are fabricated at Zentrum für Sonnenenergie- und Wasserstofforschung (ZSW) Stuttgart. More details can be found in ref. [55].

characterized by a much higher density of defects, such as Cu vacancies ( $V_{Cu}$ ) and  $In_{Cu}$  antisites, than in the GI. So, when Na diffuses back to the GB region it does not only replace Cu atoms as it is in the case of GI but it also passivates other defects.

A very intriguing result in this work is the reduction of both grain size and TB density with increasing the Na content in the CIGS absorber. The reduction in grain size with increasing the Na doping is explained by a slowing down of the GB migration during grain growth. As explained earlier, the increase in Na content implies that more Cu might be out-diffused from the bulk towards the GBs and accumulate there (but Cu content is not proportional with Na content, since Na can also passivate the defects like vacancies and antisites available in the bulk). The stronger Cu accumulation at the GBs may reduce the GB mobility during growth given that the driving force for the GB migration is to adopt a lower energy plane. This explains why the average grain size in the CIGS absorber decreases with increasing the Na content; i.e., with increasing the Cu accumulation at the GBs during growth. Moreover, the TBs, which are low-energy defects, are known to be formed when GBs are migrating given that the number of twins produced,  $D$  is proportional to the distance of migration  $d$  ( $D \sim d$ ).<sup>[45]</sup> We do not exclude here that Na might still be present at the GBs during grain growth (not all Na atoms diffused inside the grain) and have a similar effect as Cu: blocking the GB migration. Hence, the presence of Cu and eventually Na at the GBs slow down the GB migration as well as prevents the migration of steps on the GBs, thereby preventing the nucleation of twins as observed for the B dopants in Ni polycrystals.<sup>[45]</sup>

## 4.2. Deep Defects of Na Clusters as Possible Promoters for Charge Recombination

The CIGS absorber layer with a significant amount of Na dopants shows an inhomogeneous distribution of these Na atoms with significant GBs segregation and formation of Na-rich clusters inside the grains. The cluster formation is possibly attributed to the limitation in solubility of Na in CIGS and can be explained by a phase separation model in the metastable region near the solidus curve.<sup>[46]</sup> According to Rockett et al.,<sup>[47]</sup> the presence of defect complexes ( $V_{Cu}^{-1} In_{Cu}^{2+} V_{Cu}^{-1}$ )<sup>0</sup> with mutual attraction due to their dipole moments, can lead to the formation of clusters. The potential of the  $V_{Cu}^{-1}$  cluster's occupation with  $Na^{+}$  ions can explain the clustering of Na.

The formation of Na clusters at the CdS/CIGS interface has been already observed in the past.<sup>[48]</sup> Yet there, such a high quantity of Na originated from an incomplete cleaning of the CIGS surface before the deposition of CdS, especially in the connecting regions of two grains (where the presence of voids is frequently observed). Therefore, our work proves for the first time the formation of Na-rich platelet-shaped clusters when Na is found in too high quantity, due to the limited solubility of Na in the CIGS bulk. The clusters are defined using the maximum separation method of solutes,<sup>[49]</sup> by considering that the maximum distance between Na solutes is 1.5 nm and the minimum number of Na atoms in a cluster is 10. Then the average concentration of Na in these clusters is calculated. The Na clusters range between 5 and 40 nm in diameter as shown in **Figure 8**. More exactly, Figure 8a shows the 3D reconstruction map of only the Na clusters within the Na-14 sample (with the highest Na content). These clusters

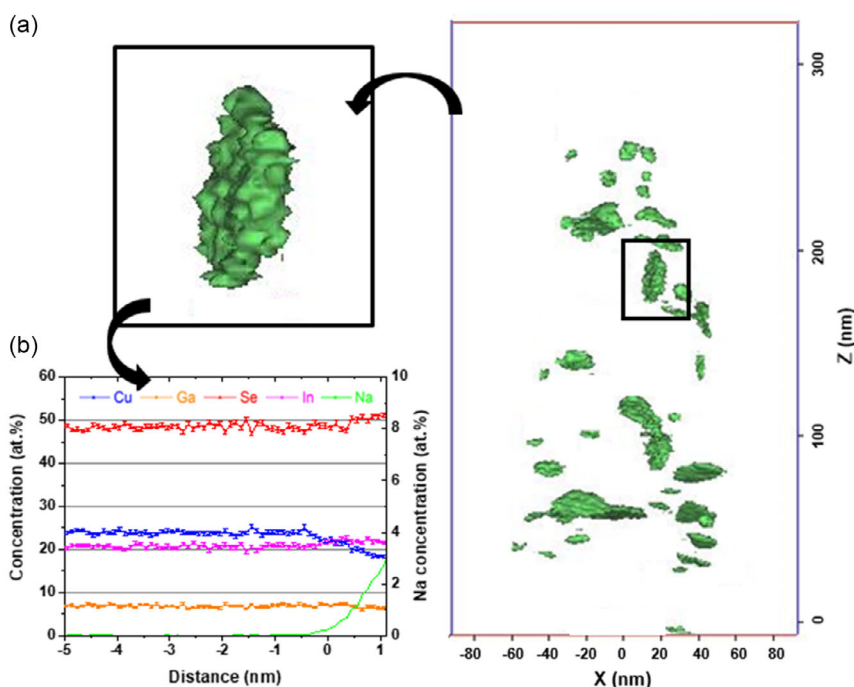


**Figure 8.** Chemical composition of cluster upon further Na addition determined by APT for the Na-14 sample. a) The clusters are visualized by an iso-composition surface made using a Na iso-composition value of 0.6 at%. b) The proxigram shows Na accumulation in the range of 2.5 at%, at the position of the zoomed-in cluster.



**Table 3.** The average composition of the Na and Cu, Ga, Se and In elements for the clusters, grain boundaries (GBs), and dislocations for the Na-14 sample. Note: The addition of the composition of all given elements and Na deviates from 100 at% since they represent the average values.

Region	Cu [at%]	In [at%]	Ga [at%]	Se [at%]	Na [at%]
Clusters	18	22.3	6.2	51.7	3
GBs	21.5	21	5.9	50.7	1.1
Dislocations	21.8	21.1	5.3	51.2	1.9

are visualized by an iso-composition surface made using a Na iso-composition value of 0.6 at%. The Proximity histogram (or proxigram)<sup>[50]</sup> in Figure 8 shows the Na composition of 2.5 at% in the zoomed-in cluster. Proxigram refers to a profile of the local atomic composition as a function of proximity to the cluster/matrix interface, where 0 nm represents the interface position. The average Na content inside these Na-rich clusters is about 3 at%, which is higher than the Na content at GBs (0.3–1 at %) and dislocations (1.8–2.1 at%; see Table 3). The average composition of In/Ga and Se are rather similar at Na-rich clusters, GBs, and dislocations, while the average Cu content inside the Na-rich clusters is much lower (18 at%) in comparison to the GBs (21.5 at%) and dislocations (21.8 at%). The composition of In, Ga, and Se elements inside the Na-rich clusters is 22.3, 6.2, and 51.7 at%, respectively.

The EBSD and APT results from Figure 5 and 6 show that the fraction of RHAGB and dislocations is increasing with increasing the Na content when going from Na-0 to Na-6. These structural defects are known to host a high fraction of both, acceptor ( $V_{Cu}^-$ ) and donor ( $In_{Cu}^{2+}$ ) defects (sometimes even as complex defects  $2V_{Cu}^- + In_{Cu}^{2+}$ <sup>[51]</sup>) and that Na may passivate these defects. Yet, the Na content at GBs (average of about 1.1 at%, see Table 3) does not fully compensate for the Cu depletion (2.46 at%) and the In enrichment (2.1 at%), which implies that these defects are still present at GBs in the Na-6 sample. The same has been observed in our recent work where the Na accumulation at the GBs does not fully compensate for the Cu-depletion and In-enrichment. For these GBs we found a preferential collection of the minority charge carriers (i.e., electrons) through electron beam-induced current studies.<sup>[30,31]</sup> We concluded hence, that these GBs are electrically charged and that the GI-GB interface is behaving like weak internal p-n junctions (weak recombination in agreement with Rau et al.<sup>[52]</sup>). This implies that GBs are positively charged dominated by the presence of donor defects such as  $In_{Cu}^{2+}$ , which is the donor defect with the lowest formation energy in the Cu-poor CIGS absorber.<sup>[53]</sup> Hence, one could also assume that the same behavior takes place for the RHAGBs for the sample Na-6.

The same arguments as described earlier can be applied when comparing the increase in defect concentration between the Na-6 and Na-14 samples; i.e., the increase in acceptor and deep defects is mainly due to the further increase of the RHAGBs fraction in the CIGS absorber as proved by EBSD. Yet, if the acceptor defect density increases with almost similar magnitudes ( $\approx$  factor 10) from one sample to the other (see Table 1), interestingly the increase in  $\Delta C$  - representing the deep defect density - between

Na-6 and Na-14 is more than two times higher than the increase in deep defect density between Na-0 and Na-6. Moreover, Kerr et al.<sup>[54]</sup> had proved using deep-level transient spectroscopy (DLTS) measurements that Na enters the In site and substitutes Cu to form  $Na_{In}$  defects, and therefore reduces the grain boundary energy barrier and removes mid-gap states (deep states). This implies that other hosts for the deep defects are present in the CIGS absorber of the Na-14 sample.

In this work, the solar cell efficiency of the Na-14 cell is noticeably smaller than the one of Na-6 despite a moderate doping increase (see Figure 2). This performance reduction originates from a drop in all device parameters. The admittance spectroscopy results show that the  $\Delta C$  assigned to deep defects is increasing with increasing Na content (see Figure 3 and 4). It may be surmised that recombination via deep defects is responsible for the device's deterioration. At this point, we think that besides the defects present at RHAGB there are other supplementary sources of possible Na-induced point defects, which are the defects in conjunction with the Na clusters. These defects can in principle trap the electrons and holes increasing the recombination in the cell as demonstrated by admittance spectroscopy.

Hence, this work elucidates the dual Na effect in the CIGS absorber. Na can segregate at GBs and act as a passivator reducing the recombination in the cell and, thus, being beneficial for the overall cell performance. Yet, when found in very high quantity in the bulk the Na starts to form clusters hosting a high concentration of deep defects and trapping the electrons within the CIGS bulk. At this stage, Na still exhibits some beneficial effects, especially in terms of bulk p-type conductivity, but at the same time presence of Na clusters in the bulk deteriorates the cell parameters proving its detrimental effect when found in too high content.

## 5. Conclusion

In this work, we investigated the dual Na effect on the structural, chemical, and electronic properties of CIGS absorbers by employing different techniques such as EBSD, APT, and AS. Previous works mainly studied the effect of Na alkali impurities on CIGS properties, which are incorporated by PDT treatment and after the deposition of the absorber layer. In this article, a new incorporation method is applied to supply Na only in quantified amounts and before the absorber layer growth by using NaF precursor layers. Extra insertion of Na and other electrically detrimental elements such as O and K is prohibited by a barrier layer between the SLG substrate and Mo. Our results clearly show that Na has a strong effect on the  $V_{OC}$  and  $V_{OC}$  deficit. The  $V_{OC}$  deficit strongly decreases as Na is added in a moderate content into the absorber. However, further addition of Na to a higher content increases the  $V_{OC}$  deficit. The structural analysis shows that the presence of a moderate content of Na optimizes the GBs properties through the Na passivation effect, while the much higher content of Na reduces the fraction of twin boundaries and grain sizes. Our APT studies confirm the EBSD results by showing a higher density of GBs, dislocations, and clusters with the highest increase of Na. We propose that these clusters are the main reason for the steep increase in deep defect concentration and the  $V_{OC}$  deficit in the samples.

## Supporting Information

Supporting Information is available from the Wiley Online Library or from the author.

## Acknowledgements

We thankfully acknowledge the funding by the German Federal Ministry for Economic Affairs and Climate Action (BMWK) within the EFFCIS-II project. This work has also been receiving funding from the DFG project SCHE 1745/7-1. [Correction added on 1 February 2024, after first online publication: Table 1 and Figure 6 were corrected.]

Open Access funding enabled and organized by Projekt DEAL.

## Conflict of Interest

The authors declare no conflict of interest.

## Data Availability Statement

The data that support the findings of this study are available from the corresponding author upon reasonable request.

## Keywords

atom-probe tomography (APT), copper indium gallium diselenide (CIGS), Cu(In, Ga)Se<sub>2</sub>, grain boundary segregation, photovoltaics, sodium diffusion, thin-film solar cells

Received: July 14, 2023

Revised: September 22, 2023

Published online: January 11, 2024

- [1] R. Kamada, T. Yagioka, S. Adachi, A. Handa, K. F. Tai, T. Kato, H. Sugimoto, in *2016 IEEE 43rd Photovoltaic Specialists Conf. (PVSC)*, Portland, OR, June 2016, pp. 1287–1291, <https://doi.org/10.1109/PVSC.2016.7749822>.
- [2] M. Krause, A. Nikolaeva, M. Maiberg, P. Jackson, D. Hariskos, W. Witte, J. A. Márquez, S. Levchenko, T. Unold, R. Scheer, D. Abou-Ras, *Nat. Commun.* **2020**, *11*, 4189.
- [3] K. Taretto, U. Rau, *J. Appl. Phys.* **2008**, *103*, 094523.
- [4] K. Taretto, U. Rau, J. H. Werner, *Thin Solid Films* **2005**, *480–481*, 8.
- [5] K. Taretto, U. Rau, *Mater. Res. Soc. Symp. Proc.* **2007**, *1012*, 309.
- [6] M. Nakamura, K. Yamaguchi, Y. Kimoto, Y. Yasaki, T. Kato, H. Sugimoto, *IEEE* **2019**, *9*, 1863.
- [7] J. Nishinaga, T. Nagai, T. Sugaya, H. Shibata, S. Niki, *Appl. Phys. Express* **2018**, *11*, 082302.
- [8] O. Cojocaru-Mirédin, M. Raghuvanshi, R. Wuerz, S. Sadewasser, *Adv. Funct. Mater.* **2021**, *31*, 2103119.
- [9] N. Nicoara, R. Manaligod, P. Jackson, D. Hariskos, W. Witte, G. Sozzi, R. Menozzi, S. Sadewasser, *Nat. Commun.* **2019**, *10*, 1.
- [10] S. Siebentritt, E. Avancini, M. Bär, J. Bombsch, E. Bourgeois, S. Buecheler, R. Carron, C. Castro, S. Duguay, R. Félix, E. Handick, D. Hariskos, V. Havu, P. Jackson, H.-P. Komsa, T. Kunze, M. Malitckaya, R. Menozzi, M. Nesladek, N. Nicoara, M. Puska, M. Raghuvanshi, P. Pareige, S. Sadewasser, G. Sozzi, A. N. Tiwari, S. Ueda, A. Vilalta-Clemente, T. P. Weiss, F. Werner, et al., *Adv. Energy Mater.* **2020**, *10*, 1903752.
- [11] P. Salomé, V. Fjällström, A. Hultqvist, M. Edoff, *IEEE J. Photovolt.* **2013**, *3*, 509.
- [12] Y. Sun, S. Lin, W. Li, S. Cheng, Y. Zhang, Y. Liu, W. Liu, *Engineering* **2017**, *3*, 452.
- [13] E. S. Mungan, X. Wang, M. A. Alam, *IEEE J. Photovolt.* **2013**, *3*, 451.
- [14] A. Laemmle, R. Wuerz, T. Schwarz, O. Cojocaru-Mirédin, P. P. Choi, M. Powalla, *J. Appl. Phys.* **2014**, *115*, 154501.
- [15] O. Cojocaru-Mirédin, P.-P. Choi, D. Abou-Ras, S. S. Schmidt, R. Caballero, D. Raabe, *IEEE J. Photovolt.* **2011**, *1*, 207.
- [16] A. Czudek, A. Urbaniak, A. Eslam, R. Wuerz, M. Igalson, *IEEE J. Photovolt.* **2020**, *10*, 1926.
- [17] A. Czudek, A. Eslam, A. Urbaniak, P. Zabierowski, R. Wuerz, M. Igalson, *J. Appl. Phys.* **2020**, *128*, 173102.
- [18] V. Bhatt, S.-T. Kim, M. Kumar, H.-J. Jeong, J. Kim, J.-H. Jang, J.-H. Yun, *Thin Solid Films* **2023**, *767*, 139673.
- [19] R. Caballero, C. A. Kaufmann, T. Eisenbarth, T. Unold, S. Schorr, R. Hesse, R. Klenk, H.-W. Schock, *Phys. Status Solidi A: Appl. Mater. Sci.* **2009**, *206*, 1049.
- [20] M. Theelen, N. Barreau, V. Hans, H. Steijvers, Z. Vroon, M. Zeman, in *2015 IEEE 42nd Photovoltaic Specialist Conf. (PVSC)*, New Orleans, LA, June 2015, pp. 1–6, <https://doi.org/10.1109/PVSC.2015.7355776>.
- [21] Y. Wang, S. Lv, Z. Li, J. Mater. Sci. Technol. **2022**, *96*, 179.
- [22] S. Ishizuka, A. Yamada, K. Matsubara, P. Fons, K. Sakurai, S. Niki, *Curr. Appl. Phys.* **2010**, *10*, S154.
- [23] D.-H. Cho, K.-S. Lee, Y.-D. Chung, J.-H. Kim, S.-J. Park, J. Kim, *Appl. Phys. Lett.* **2012**, *101*, 23901.
- [24] S.-H. Wei, S. B. Zhang, A. Zunger, *J. Appl. Phys.* **1999**, *85*, 7214.
- [25] J. Matsuura, I. Khatri, T.-Y. Lin, M. Sugiyama, T. Nakada, *Prog. Photovolt. Res. Appl.* **2019**, *27*, 623.
- [26] A. M. Gabor, J. R. Tuttle, D. S. Albin, M. A. Contreras, R. Noufi, A. M. Hermann, *Appl. Phys. Lett.* **1994**, *65*, 198.
- [27] K. Thompson, D. Lawrence, D. J. Larson, J. D. Olson, T. F. Kelly, B. Gorman, *Ultramicroscopy* **2007**, *107*, 131.
- [28] O. Cojocaru-Mirédin, L. Abdellou, M. Nagli, S. Zhang, Y. Yu, C. Scheu, D. Raabe, M. Wuttig, Y. Amouyal, *ACS Appl. Mater. Interfaces* **2017**, *9*, 14779.
- [29] M. Raghuvanshi, M. Chugh, G. Sozzi, A. Kanevce, T. D. Kühne, H. Mirhosseini, R. Wuerz, O. Cojocaru-Mirédin, *Adv. Mater.* **2022**, *34*, 2203954.
- [30] M. Raghuvanshi, B. Thöner, P. Soni, M. Wuttig, R. Wuerz, O. Cojocaru-Mirédin, *ACS Appl. Mater. Interfaces* **2018**, *10*, 14759.
- [31] M. Raghuvanshi, R. Wuerz, O. Cojocaru-Mirédin, *Adv. Funct. Mater.* **2020**, *30*, 1.
- [32] R. Scheer, H.-W. Schock, *Chalcogenide Photovoltaics*, Wiley-VCH, Berlin.
- [33] F. Oberegner, N. Barreau, W. Witte, R. Scheer, *J. Appl. Phys.* **2015**, *117*, 55704.
- [34] T. Schneider, C. Dethloff, T. Hölscher, H. Kempa, R. Scheer, *Prog. Photovolt. Res. Appl.* **2022**, *30*, 191.
- [35] J. Heath, P. Zabierowski, *Advanced Characterization Techniques for Thin Film Solar Cells*, Wiley-VCH Verlag GmbH & Co. KGaA, Weinheim **2011**, p. 81, <https://doi.org/10.1002/9783527636280.ch4>.
- [36] T. Maeda, A. Kawabata, T. Wada, *Jpn. J. Appl. Phys.* **2015**, *54*, 08KC20.
- [37] D. Rudmann, G. Bilger, M. Kaelin, F.-J. Haug, H. Zogg, A. N. Tiwari, *Thin Solid Films* **2003**, *431–432*, 37.
- [38] J. H. Yun, K. H. Kim, M. S. Kim, B. T. Ahn, S. J. Ahn, J. C. Lee, K. H. Yoon, *Thin Solid Films* **2007**, *515*, 5876.
- [39] R. Caballero, C. A. Kaufmann, T. Eisenbarth, M. Cancela, R. Hesse, T. Unold, A. Eicke, R. Klenk, H. W. Schock, *Thin Solid Films* **2009**, *517*, 2187.
- [40] O. Cojocaru-Mirédin, T. Schwarz, D. Abou-Ras, *Scr. Mater.* **2018**, *148*, 106.
- [41] T. Schwarz, G. Stechmann, B. Gault, O. Cojocaru-Mirédin, R. Wuerz, D. Raabe, *Prog. Photovolt. Res. Appl.* **2018**, *26*, 196.

- [42] M. Raghuwanshi, J. Keutgen, A. M. Mio, H. Mirhosseini, T. D. Kühne, O. Cojocar-Mirédin, *Sol. RRL* **2023**, *7*, 2201033.
- [43] O. Cojocar-Mirédin, P. Choi, R. Wuerz, D. Raabe, *Ultramicroscopy* **2011**, *111*, 552.
- [44] Z. K. Yuan, S. Chen, Y. Xie, J.-S. Park, H. Xiang, X.-G. Gong, S.-H. Wei, *Adv. Energy Mater.* **2016**, *6*, 1.
- [45] C. S. Pande, M. A. Imam, *Mater. Sci. Eng. A* **2009**, *512*, 82.
- [46] P.-P. Choi, O. Cojocar-Mirédin, R. Wuerz, D. Raabe, *J. Appl. Phys.* **2011**, *110*, 124513.
- [47] A. Rockett, *Thin Solid Films* **2000**, *361–362*, 330.
- [48] O. Cojocar-Mirédin, P. Choi, R. Wuerz, D. Raabe, *Appl. Phys. Lett.* **2012**, *101*, 181603.
- [49] D. Vaumousse, A. Cerezo, P. J. Warren, *Ultramicroscopy* **2003**, *95*, 215.
- [50] O. C. Hellman, J. A. Vandenbroucke, J. Rüsing, D. Isheim, D. N. Seidman, *Microsc. Microanal.* **2000**, *6*, 437.
- [51] D. Colombara, H. Elanzeery, N. Nicoara, D. Sharma, M. Claro, T. Schwarz, A. Koprek, M. H. Wolter, M. Melchiorre, M. Sood, N. Valle, O. Bondarchuk, F. Babbe, C. Spindler, O. Cojocar-Mirédin, D. Raabe, P. J. Dale, S. Sadewasser, S. Siebentritt, *Nat. Commun.* **2020**, *11*, 3634.
- [52] U. Rau, K. Taretto, S. Siebentritt, *Appl. Phys. A* **2009**, *96*, 221.
- [53] C. Persson, Y.-J. Zhao, S. Lany, A. Zunger, *Phys. Rev. B* **2005**, *72*, 035211.
- [54] L. L. Kerr, S. S. Li, S. W. Johnston, T. J. Anderson, O. D. Crisalle, W. K. Kim, J. Abushama, R. N. Noufi, *Solid State Electron.* **2004**, *48*, 1579.
- [55] H. Luo, A. Karami, H. Mirhosseini, R. Wuerz, W. Witte, O. Cojocar-Mirédin, *J. Appl. Phys.* **2023**, in preparation.